HHS Public Access

Author manuscript

Neuromuscul Disord. Author manuscript; available in PMC 2016 October 01.

Published in final edited form as:

Neuromuscul Disord. 2015 October ; 25(10): 764–772. doi:10.1016/j.nmd.2015.07.003.

Abnormalities in brain structure and biochemistry associated with *mdx* mice measured by *in vivo* MRI and high resolution localized ^{1}H MRS

Su Xu[1], **Da Shi**[1], **Stephen J.P. Pratt**[2], **Wenjun Zhu**[1], **Andrew Marshall**[1], and **Richard M. Lovering**[2]

[1]Department of Diagnostic Radiology and Nuclear Medicine, University of Maryland School of Medicine, USA

[2]Department of Orthopaedics, University of Maryland School of Medicine, USA

Abstract

Duchenne muscular dystrophy (DMD), an X-linked disorder caused by the lack of dystrophin, is characterized by the progressive wasting of skeletal muscles. To date, what is known about dystrophin function is derived from studies of dystrophin-deficient animals, with the most common model being the *mdx* mouse. Most studies on patients with DMD and in *mdx* mice have focused on skeletal muscle and the development of therapies to reverse, or at least slow, the severe muscle wasting and progressive degeneration. However, dystrophin is also expressed in the CNS. Both *mdx* mice and patients with DMD can have cognitive and behavioral changes, but studies in the dystrophic brain are limited. We examined the brain structure and metabolites of mature wild type (WT) and *mdx* mice using magnetic resonance imaging and spectroscopy (MRI/MRS). Both structural and metabolic alterations were observed in the *mdx* brain. Enlarged lateral ventricles were detected in *mdx* mice when compared to WT. Diffusion tensor imaging revealed elevations in diffusion diffusivities in the prefrontal cortex and a reduction of fractional anisotropy in the hippocampus. Metabolic changes included elevations in phosphocholine and glutathione, and a reduction in γ-aminobutyric acid in the hippocampus. In addition, an elevation in taurine was observed in the prefrontal cortex. Such findings indicate a regional structural change, altered cellular antioxidant defenses, a dysfunction of GABAergic neurotransmission, and a perturbed osmoregulation in the brain lacking dystrophin.

Keywords

skeletal muscle; dystrophy; DMD; magnetic resonance spectroscopy; magnetic resonance imaging; diffusion tensor imaging

Correspondence to: Dr. Rich Lovering, University of Maryland, School of Medicine, Department of Orthopaedics, AHB, Rm 540, 100 Penn St., Baltimore, MD 21201, USA, phone: 410-706-2417, fax: 410-706-0028, rlovering@som.umaryland.edu.

Introduction

Duchenne muscular dystrophy (DMD) is an X-linked muscle disorder characterized clinically by severe, progressive and irreversible muscle wasting and loss of muscular function [1–3]. This devastating and fatal disease is due to the lack of dystrophin, a large membrane-associated protein expressed in striated muscle and localized to the inner face of the sarcolemma [4;5]. The *mdx* mouse, the most common animal model for DMD, also lacks dystrophin and shares much of the muscle pathology found in DMD patients. Despite the wealth of studies describing the role of dystrophin in muscle, there has been relatively little progress in developing disease therapies.

In addition to the well-described muscle wasting phenomenon, it is generally accepted that some patients with DMD have cognitive impairments. In the original description of the disease circa 1861, Duchenne reported 5 patients with some degree of cognitive defects [6]. Since then, an overwhelming amount of evidence has shown that there can be a significant cognitive impairment in DMD patients [7;8]; mental retardation affects around 30% of boys with DMD [9]. Impaired memory function, especially restricted verbal short term memory, seems to characterize the neuropsychological profile of many patients with DMD [10;11]. Language impairments, long-term memory problems, and limited executive functions have also been reported [9;12–14]. For *mdx* mice, behavioral studies have also shown impairments in learning as tested in several paradigms [15–17].

The presence of the cognitive dysfunction raises the question of neuropathology. Both CT and *in vivo* ^{1}H MRS studies [18–20] suggest a slow, progressive cerebral degeneration in the DMD patients. Clear signs of cortical atrophy and ventricular dilation were observed in CT images in older patients, and patients with large amounts of physical disability [18]. Using ^{1}H MRS, Rae et al. [20] showed significant increases in ratios of choline-containing compounds to *N*-acetylaspartate (tCho/NAA) and tCho/creatine (Cr) in the cerebellum in DMD boys compared to age-matched normal boys. Within the DMD group, the abnormal tCho/NAA group was significantly older (mean age: 12 years) than the normal tCho/NAA group (mean age: 8 years), which reflects the progressive nature of the disease. In contrast, a localized *in vivo* ^{1}H MRS study by Kreis et al. [21] showed a significant decrease in absolute tCho levels in both the cerebellum and the temporo-parietal cortex the DMD patients (mean age: 12 years). Very few studies have explored *in vivo* ^{1}H MRS on *mdx* mice. In an early non-localized *in vivo* ^{1}H MRS study, there were significantly low ratios of Cr/tCho and NAA/tCho in *mdx* brains compared to controls at the age between 2 and 5 months [22].

Dystrophin, normally expressed in the post-synaptic neuronal terminals of the cortex, hippocampus and cerebellum areas, is involved with reasoning and learning [23] and is completely or partially absent in DMD patients, as well as in the genetically homologous *mdx* mice [24;25]. This suggests that a cognitive impairment may be the result of the missing protein; however the precise function of dystrophin in brain is still unknown. In the muscle, it has been suggested that dystrophin plays both functional and structural roles such as: supporting the sarcolemma against mechanical stress and stabilizing it in the course of contraction–relaxation cycles [26]; taking part in the regulation of intracellular calcium and

the cascade of calcium-related events [27;28]; working in force and signal transduction [29]; influencing the aggregation of neurotransmitter receptors [30;31]; and preventing excessive generation of reactive oxygen free radical species [32;33]. Some of these mechanisms may also be applicable in the brain. Identifying the role of dystrophin in the brain would be extremely helpful as effective therapies are developed for DMD.

In this study, we used *in vivo* magnetic resonance imaging (MRI), high resolution localized magnetic resonance spectroscopy (^{1}H MRS), and *ex vivo* diffusion tensor imaging (DTI) to investigate alterations in brain structure (MRI and DTI) and metabolites (MRS) from mature *mdx* mouse brains. The use of *in vivo* MRI will not only be helpful in elucidating dystrophin function in the brain, but also for continuing development of non-invasive tools for use in diagnosis, disease progression and even drug therapy. As non-invasive technology continues to improve and imaging such as MRI/MRS becomes more commonplace, these tools will play a greater role in diagnosis, prognosis, and in rehabilitation planning.

Materials and Methods

Eight male dystrophic mice (*mdx*, C57BLScSn-DMD*mdx*, approximately 9 months old) and seven male aged-matched wild type mice (WT, C57BL/10ScSn) were obtained from Jackson Laboratory, Bar Harbor, ME. The MRI and MRS acquisitions were performed on mice close to one year of age. The experiments were performed on a Bruker BioSpec 70/30USR Avance III 7T scanner. A Bruker four-element ^{1}H surface coil array was used as the receiver and a Bruker 72 mm linear-volume coil as the transmitter. Each mouse was anesthetized in an animal chamber using a gas mixture of O_2 (1 L/min) and isoflurane (3 %) then later maintained at 1–1.5% isoflurane during scanning. An MR compatible small-animal monitoring system was used to monitor the animal respiration rate and body temperature. The animal body temperature was maintained at 36–37°C using warm water circulation.

Both proton-density-weighted and T_2-weighted images were obtained using a 2D rapid acquisition with relaxation enhancement (RARE) sequence in the axial plane (repetition time (TR)/echo time $(TE)_{eff1}/TE_{eff2}$ = 5500/19/58 msec, RARE factor = 4, field of view (FOV) = 20 × 20 mm^2, slice thickness = 1 mm, in-plane resolution = 114 × 114 μm^2, number of averages (NA) = 1). A fluid-attenuated inversion recovery (FLAIR) pulse sequence (TR/Inversion time/TE = 10000/1600/48 ms, in-plane resolution = 78 × 78 μm^2, other parameters were the same as T_2-weighted images) was performed on 3 WT and 5 *mdx* mice to confirm the dilution of the ventricles, which was found in the T_2-weighted MRI examination, and to check the potential periventricular hyperintense lesions in *mdx* mice. Volumetric analysis was measured by hand-drawing a region of interest with the Medical Image Processing, Analysis and Visualization tool (MIPAV v5.3.1, CIT; NIH, Bethesda, MD, USA). An atlas of mouse brain anatomy [34] was used for identifying structural boundaries. Nine consecutive slices were used for the volumetric analysis of the brain. The first slice was set at the beginning of the cerebrum (interaural 7.36 mm and bregma 3.56), which did not include the olfactory bulb. The slice prior to the opening of the cerebellum was (interaural −1.04 mm and bregma −4.84 mm) defined as the last slice. Brain ventricles were included in measuring brain tissue volume.

A short-TE Point-RESolved Spectroscopy (PRESS) pulse sequence [35] (TR/TE = 2500/10 ms, NA = 600) was used for MRS data acquisition with the voxel centered on the prefrontal cortex (PFC, 1.8 × 1.8 × 1.8 mm^3), hippocampus (HP, 1.5 × 6.0 × 1.5 mm^3), and cerebellum (CB, 1.4 × 4 × 1.5 mm^3), respectively (Figure 1A). The unsuppressed water signal from each of the prescribed voxels was obtained to serve as a reference for determining the specific metabolite concentrations. Quantification of the MRS was based on frequency domain analysis using a "Linear Combination of Model spectra" (LCModel)[36]. Absolute concentrations were estimated with the LCModel automatic procedure.

After all the *in vivo* MR procedures, mice were anesthetized with 4% isoflurane and then perfused through the left ventricle with 1 × phosphate buffered saline (PBS) and followed by 4% paraformaldehyde. The whole brain was removed from the skull and stored in PBS. The fixed brain was placed in a customized conical tube filled with Fluorinert (3M, St. Paul, MN) that decreased background during *ex vivo* MRI experiments. The anatomical images were taken from a 3-dimentional (3D) RARE T_2-weighted sequence (TR/TE_{eff} = 2500/33 ms, RARE factor = 8, FOV = 12 × 18 × 14 mm^3, isotopically spatial resolution = 150 μm^3, NA=2). DTI images were acquired with a 3D multiple shots, spin-echo echo-planar imaging (EPI) sequence (TR/TE = 500/30.95 ms, number of segments = 4, gradient directions = 64, diffusion gradient on time = 4 ms, temporal spacing time = 20 ms, NA=1, the FOV and spatial resolution were the same as T_2-weighted images). Two b-values (2000 and 4000 s/mm^2) were acquired for each direction following the acquisition of 5 images acquired with b = 0 s/mm^2. DTI reconstruction was performed on each voxel using in-house MATLAB program (Mathworks, Natick, MA), as described [37]. The regions of interest for the DTI experiments were drawn manually with FSLview (Analysis Group, FMRIB, Oxford, UK) including PFC, HP, cerebellum white matter, and cerebellum grey matter (Figure 1B). Maps of mean diffusivity (MD) which measures the average water diffusion within the brain tissue, axial diffusivity (AD) which measures the water diffusion along the neuronal axons, radial diffusivity (RD) which measures the water diffusion perpendicular to the axons, and fractional anisotropy (FA) which measures the degree of diffusion anisotropy of the brain tissue were generated.

After imaging, several brains were then processed for histology (WT and *mdx*, N=2 each). Samples were dehydrated with 30% sucrose for 1 week. Samples were placed in a cryostat at −19°C for 5 min, mounted using OCT mounting medium, and sectioned at 40 μm from anterior to posterior, through the hippocampus. Sections were stored at −20 °C in cryo-protectant until processed for histology. Qualitative histological comparison of brain sections to MRI were made with sections selected based on similar anatomical landmarks such as the corpus callosum and the caudate putamen using a mouse brain atlas [38]. Sections were mounted in PBS, coversliped and imaged using a Nikon Eclipse 50i microscope and Nikon's NIS-Elements Basic Research software to create a stitched image (10× objective). Volumetric analysis was not performed as was done for the imaging.

All experimental procedures were approved by the University of Maryland School of Medicine Institutional Animal Care and Use Committee. MRI and MRS results from *mdx* and WT mice were compared using independent student's t-test.

Results

The *mdx* mice showed obviously enlarged lateral ventricles on both T_2-weighted (Fig. 2A) and FLAIR images (Fig. 2B) and this finding was confirmed by volumetric measurements (Fig. 2C); (despite no differences in total brain tissue volume, lateral ventricle volume/brain tissue volume ratios were: WT [0.034 ± 0.003] vs. *mdx* [0.066 ± 0.005], p = 0.0001). The enlarged ventricles are likely caused by grey matter atrophy, although we cannot rule out compression from excess cerebrospinal fluid (CSF), which was displayed by the high signal intensity (bright white) on the coronal T_2-weighed images (Fig. 2A) and low signal intensity (dark black) on the coronal FLAIR images (Fig. 2B). No obvious periventricular hyper-intense lesions were detected on the *mdx* mice by the FLAIR images. When comparing brain tissue volume, there was no significant difference between the whole brain tissue volume (mm^3)/body weight (g) ratios between WT (8.861 ± 0.196) and *mdx* (9.287 ± 0.397, p=0.380). Representative histology confirmed enlarged ventricles in the *mdx* brain when compared to WT (Fig. 3).

DTI results demonstrated significant elevations in MD, AD, and RD in the PFC of *mdx* mice when compared to WT (Fig. 4, $p < 0.05$). These data indicate a more continuous movement of water molecules with less restrictions and boundaries. There was also a significant decrease in FA in HP ($p < 0.05$), indicating a low density of the ordered tissue in *mdx* mice. There were no statistical differences in DTI measurements for both white and grey matter in the CB (data not shown).

Representative high resolution localized *in vivo* MRS spectra from the HP of the two groups of mice are shown in Fig. 5. The following neurochemicals were observed: Creatine (Cr), γ-aminobutyric acid (GABA), glutamate (Glu), glutamine (Gln), glycerophosphocholine (GPC), glutathione (GSH), *myo*-inositol (Ins), *N*-acetyl-aspartate (NAA), *N*-acetylaspartylglutamate (NAAG), phosphocholine (PCh), phosphocreatine (PCr), taurine (Tau), total Creatine (tCr) = Cr+ PCr, total Choline (tCho) = GPC + PCh, and glutamate/glutamine complex (Glx =Glu +Gln). Compared to WT mice, *mdx* mice demonstrated a significant elevation in Tau ($p < 0.05$) in the PFC, and a decrease in GABA ($p < 0.01$) as well as significant elevations in PCh ($p < 0.05$) and GSH ($p < 0.05$) in the HP (Fig. 6). No differences were observed in other metabolites from these two regions. There were no significant alterations of the metabolites in the CB (data not shown).

Discussion

To the best of our knowledge, this is the first study to demonstrate that the combination of MRI and ^1H MRS can detect alterations in structure (MRI and DTI) and metabolism (MRS) in mature *mdx* mouse brains. The structural alterations seen in *mdx* mice included a macro level change (ventricular dilation) and micro level changes (increased water diffusivity and decreased anisotropy in cells). The alterations in metabolite concentrations in *mdx* mouse brains occurred in the HP and PFC regions, where dystrophin is typically expressed in WT mice. Significant elevations in Tau (in PFC), GSH (in HP), PCh (in HP) and a significant reduction in GABA (in HP) were observed in *mdx* mice. An imbalance in these metabolites

has implications for dystrophin functions such as osmoregulation, oxidative stress, membrane phospholipid synthesis, and GABAergic neurotransmission in the brain.

In addition to its mechanical function, the dystrophin-associated protein complex (DAPC) could act as a transmembrane signaling complex [39;40]. Further complicating matters, the dystrophin gene also has several internal promoters throughout the gene that give rise to shorter dystrophin proteins; some of these specific isoforms of dystrophin are exclusively, or predominantly, expressed in the brain [41;42]. The function(s) of dystrophin in the brain remains to be elucidated. Recent studies suggest a possible relationship between exists between certain mutations or loss of specific isoforms and cognitive impairment in DMD patients [43–46], but this is difficult to prove until all brain dystrophin isoforms are fully understood [47].

Dystrophin is found in the soma and dendrites of cortical and hippocampal pyramidal neurons, and in cerebellar Purkinje cells [48]. Little if any dystrophin reactivity is detected in striatum, thalamus, hypothalamus and brain stem [48]. Dystrophin is associated with the post-synaptic membrane of neurons and is present at high levels in post-synaptic dendrites, suggesting that it might have a role in synapse structure or/and interneuronal transmission [48;49]. In muscle, the uniform distribution of dystrophin beneath the plasma membrane is thought to provide structural support to the membrane. In the *mdx* mouse brain, the blood-brain barrier (BBB) is markedly altered due to disruption of tight junctions, leading to increased permeability in the BBB [50;51]. Although its role in the brain is still being defined, the absence of dystrophin may enable water in the cell to diffuse more easily and less anisotropically, as indicated by DTI results of the current study (i.e. increased MD, AD, RD, and a decreased FA).

Tau is an atypical amino acid that is required for proper development and function of skeletal muscle [52;53]. Tau is a hydrolyte attributed to efficiently transporting potassium, sodium, and calcium (Ca^{2+}) in and out of the cell [54]. It is also known to play a significant role in many physiological activities, including maintaining a stable, constant condition of Ca^{2+} in the brain tissue. Studies have shown that Ca^{2+} homeostasis is perturbed in *mdx* muscle [33;55–57], elevations are seen in skeletal muscle at all ages in *mdx* mice. The high level of Tau in the mature *mdx* brain may indicate a perturbed Ca^{2+} homeostasis in the PFC. Such a role would be tantamount to the altered calcium handling observed in skeletal muscle when dystrophin is missing [28;33;55;58–61].

GSH is an antioxidant, and antioxidants play a role in preventing damage to cells caused by reactive oxygen species (ROS). The high level of GSH we observed in *mdx* mice may be compensatory due to high levels of glutathione reductase, glutathione peroxidase, and glutathione S-transferases, as reported in both patients with muscular dystrophy [62] and in homologous animal models such as dystrophic chickens [63;64]. The increase in GSH might indicate altered cellular antioxidant defenses in the HP in the mature *mdx* mice.

Elevated concentrations of choline-containing compounds has previously been reported in extracts of whole brain (60–150 days old) [22] and in the HP and CB (> 6 months old) in *mdx* mice [65]. More specifically, our current *in vivo* study demonstrated an elevated

concentration of PCh in HP. The alteration of the PCh level may be a result of oxidative modification in the *mdx* mouse brains. It has been reported that there is a significant decrease in the level of phosphocholine-hydrolyzing activity, which decreases the conversion of phosphocholine into choline in brains of Alzheimer's disease patients [66]. An elevated phosphocholine level was found early in Alzheimer's pathogenesis [67]. The decrease in the level of phosphocholine-hydrolyzing activity has been suggested to be caused by the oxidative inactivation of the related enzymes through oxidant radicals [68]. One of the hypothesized functions of dystrophin in muscle is to prevent excessive generation of reactive oxygen free radical species [33;69]. The ultimate effect from the lack of dystrophin and resulting differences in the levels of GSH and PCh between the WT and *mdx* mice in the HP is still not clear.

The reduction in GABA in the HP may indicate a dysfunction of GABAergic neurotransmission in the *mdx* mice. Knuesel et al. [70] found co-localization of the $GABA_A$ channel with dystrophin in the mouse HP and CB. The number of $GABA_A$ clusters in *mdx* mice was reduced by 50% in these regions. However, in the cerebral cortex, where dystrophin clusters and $GABA_A$ clusters are normally separated, no reduction of $GABA_A$ clusters was detected. The reduction in $GABA_A$ in the HP adds evidence showing that dystrophin influences the aggregation of neurotransmitter receptors [30;31;70].

In our current study, no structural and metabolic alterations were detected in the CB of *mdx* mice, a region normally expressing dystrophin. The reason for this is unknown and warrants further investigation. Indeed, dystrophin is present in neurons in a very restricted distribution, both in terms of cell type and subcellular location. It is possible that dystrophin may play different roles in different regions. As such, it may not be surprising that despite the consistent lack of dystrophin our findings are restricted to the PFC and HP. Interestingly, these are the brain regions most strongly associated with cognitive function. Given the limited distribution of dystrophin, it is also not surprising that only mild cognitive dysfunction characterizes DMD and *mdx*. The major clinical issue in DMD is the skeletal muscle dysfunction, and this has understandably received the greatest attention. There has been very little clinical investigation of the role of dystrophin in the CNS in DMD. In the current study, we report enlarged lateral ventricles, changes in DTI parameters, elevations in GSH and PCh, and a reduction in GABA in the HP corresponding to an elevation in Tau in the PFC. Such findings indicate a regional structural change, altered cellular antioxidant defenses, a dysfunction of GABAergic neurotransmission, and a perturbed osmoregulation in the brain lacking dystrophin.

The use of *in vivo* MRI/MRS has shown to be helpful in elucidating dystrophin's function in the brain in the current study. These technologies could be expanded for continuing development of non-invasive tools for use in diagnosis, monitoring disease progression, and even drug therapy outcomes. Restoration of dystrophin expression in the brain is the ideal therapeutic goal. A recently developed class of antisense oligonucleotides made of tricyclo-DNA (tcDNA-AONs) is showing promise in restoring dystrophin to levels necessary for a life-changing therapy for patients with DMD. A recent study has shown that systemic delivery of tcDNA-AONs promotes a high degree of rescue of dystrophin expression in skeletal muscles, the heart and, to a lesser extent, the brain in *mdx* mice [71]. The

neuroimaging methods used in the current study can be used to noninvasively monitor the efficiency of this potential therapeutic agent in both patient and animals. It is now clear that therapeutic studies in *mdx* mice should not simply focus on muscle, but should include other tissues such as brain.

The current study extends our understanding the dystrophin function in brain, but has several limitations. First, we are using an animal model of DMD. Much of what is known about dystrophin structure-function in muscles is derived from studies of dystrophin-deficient animals, with the most common model being the *mdx* mouse. The DMD and the *mdx* conditions are similar in that dystrophin is missing from all tissues, however, the absence of dystrophin is not equally damaging to muscles of patients with DMD and *mdx* mice; the *mdx* phenotype is much less severe than that seen with DMD. Second, the data we generated represent only one time point. A “critical period” has been described for the *mdx* mouse, during which there is a peak in muscle weakness, myofiber necrosis and regeneration between the 2^{nd} and 5^{th} weeks of life [72–76]. It is not known if such changes in severity also occur in the brain over time. Third, it is not clear if patients with DMD have consistent gross or histological abnormalities of the brain. Available studies show conflicting results, from no change in brain weight or gross histology [20;77;78] to marked brain abnormalities [79–82], including ventricular dilation [18;83;84]. Fourth, we have a relatively small sample size for all the experiments and the corresponding histological sections were not quantified. Finally, the enzyme glutamic acid decarboxylase responsible for GABA levels (Gad) is known to be deficient in the background of mice used (C57BLScSn) [85], which alters synaptic clustering of GABA receptors [65;86] in this strain. Despite the differences measured between mice of the same strain, it is not known if mice with healthy Gad/GABA activity show the same results as found here. One way to address this question would be to perform these same experiments in *mdx* mice of a different background, such as the exon 52–deleted *mdx* (*mdx*52) mouse.

In summary, we studied the structure and metabolites of healthy and dystrophic mouse brains with MRI/MRS and found in dystrophic brains: enlarged lateral ventricles, alterations in diffusion of the prefrontal cortex and hippocampus, and several metabolic alterations.

Acknowledgments

Grants: This work was supported by grants to RML (R01AR059179) from National Institutes of Health (NIH).

References

1. McDonald CM, Abresch RT, Carter GT, et al. Profiles of neuromuscular diseases. Duchenne muscular dystrophy. Am J Phys Med Rehabil. 1995; 74:S70–S92. [PubMed: 7576424]
2. Brooke MH, Fenichel GM, Griggs RC, et al. Duchenne muscular dystrophy: patterns of clinical progression and effects of supportive therapy. Neurology. 1989; 39:475–481. [PubMed: 2927672]
3. Lovering RM, Porter NC, Bloch RJ. The muscular dystrophies: from genes to therapies. Phys Ther. 2005; 85:1372–1388. [PubMed: 16305275]
4. Tinsley JM, Blake DJ, Zuellig RA, Davies KE. Increasing complexity of the dystrophin-associated protein complex. Proc Natl Acad Sci U S A. 1994; 91:8307–8313. [PubMed: 8078878]
5. Blake DJ, Tinsley JM, Davies KE. Utrophin: a structural and functional comparison to dystrophin. Brain Pathol. 1996; 6:37–47. [PubMed: 8866746]

6. Duchenne, G. I'Electrisation Localisee at de son Application a la Pathologie at a la Therapeutique. Paris: Bailliere et Fils; 1861.
7. Anderson JL, Head SI, Rae C, Morley JW. Brain function in Duchenne muscular dystrophy. Brain. 2002; 125:4–13. [PubMed: 11834588]
8. Nardes F, Araujo AP, Ribeiro MG. Mental retardation in Duchenne muscular dystrophy. J Pediatr (Rio J). 2012; 88:6–16. [PubMed: 22344614]
9. Cotton SM, Voudouris NJ, Greenwood KM. Association between intellectual functioning and age in children and young adults with Duchenne muscular dystrophy: further results from a meta-analysis. Dev Med Child Neurol. 2005; 47:257–265. [PubMed: 15832549]
10. Hinton VJ, Fee RJ, Goldstein EM, De Vivo DC. Verbal and memory skills in males with Duchenne muscular dystrophy. Dev Med Child Neurol. 2007; 49:123–128. [PubMed: 17254000]
11. Wingeier K, Giger E, Strozzi S, et al. Neuropsychological impairments and the impact of dystrophin mutations on general cognitive functioning of patients with Duchenne muscular dystrophy. J Clin Neurosci. 2011; 18:90–95. [PubMed: 21109441]
12. Cotton S, Voudouris NJ, Greenwood KM. Intelligence and Duchenne muscular dystrophy: full-scale, verbal, and performance intelligence quotients. Dev Med Child Neurol. 2001; 43:497–501. [PubMed: 11463183]
13. Wicksell RK, Kihlgren M, Melin L, Eeg-Olofsson O. Specific cognitive deficits are common in children with Duchenne muscular dystrophy. Dev Med Child Neurol. 2004; 46:154–159. [PubMed: 14995084]
14. Marini A, Lorusso ML, D'Angelo MG, et al. Evaluation of narrative abilities in patients suffering from Duchenne Muscular Dystrophy. Brain Lang. 2007; 102:1–12. [PubMed: 17428527]
15. Muntoni F, Mateddu A, Serra G. Passive avoidance behaviour deficit in the mdx mouse. Neuromuscul Disord. 1991; 1:121–123. [PubMed: 1822782]
16. Perronnet C, Chagneau C, Le BP, et al. Upregulation of brain utrophin does not rescue behavioral alterations in dystrophin-deficient mice. Hum Mol Genet. 2012; 21:2263–2276. [PubMed: 22343141]
17. Vaillend C, Rendon A, Misslin R, Ungerer A. Influence of dystrophin-gene mutation on mdx mouse behavior. I. Retention deficits at long delays in spontaneous alternation and bar-pressing tasks. Behav Genet. 1995; 25:569–579. [PubMed: 8540895]
18. Yoshioka M, Okuno T, Honda Y, Nakano Y. Central nervous system involvement in progressive muscular dystrophy. Arch Dis Child. 1980; 55:589–594. [PubMed: 7436514]
19. Chen DH, Takeshima Y, Ishikawa Y, Ishikawa Y, Minami R, Matsuo M. A novel deletion of the dystrophin S-promoter region cosegregating with mental retardation. Neurology. 1999; 52:638–640. [PubMed: 10025804]
20. Rae C, Scott RB, Thompson CH, et al. Brain biochemistry in Duchenne muscular dystrophy: a 1H magnetic resonance and neuropsychological study. J Neurol Sci. 1998; 160:148–157. [PubMed: 9849797]
21. Kreis R, Wingeier K, Vermathen P, et al. Brain metabolite composition in relation to cognitive function and dystrophin mutations in boys with Duchenne muscular dystrophy. NMR Biomed. 2011; 24:253–262. [PubMed: 21404337]
22. Tracey I, Dunn JF, Parkes HG, Radda GK. An in vivo and in vitro H-magnetic resonance spectroscopy study of mdx mouse brain: abnormal development or neural necrosis? J Neurol Sci. 1996; 141:13–18. [PubMed: 8880686]
23. Cyrulnik SE, Hinton VJ. Duchenne muscular dystrophy: a cerebellar disorder? Neurosci Biobehav Rev. 2008; 32:486–496. [PubMed: 18022230]
24. Tracey I, Dunn JF, Radda GK. Brain metabolism is abnormal in the mdx model of Duchenne muscular dystrophy. Brain. 1996; 119 (Pt 3):1039–1044. [PubMed: 8673481]
25. Uchino M, Yoshioka K, Miike T, et al. Dystrophin and dystrophin-related protein in the brains of normal and mdx mice. Muscle Nerve. 1994; 17:533–538. [PubMed: 8159184]
26. Koenig M, Monaco AP, Kunkel LM. The complete sequence of dystrophin predicts a rod-shaped cytoskeletal protein. Cell. 1988; 53:219–228. [PubMed: 3282674]
27. Lansman JB, Franco A Jr. What does dystrophin do in normal muscle? J Muscle Res Cell Motil. 1991; 12:409–411. [PubMed: 1658040]

28. Lovering RM, Michaelson L, Ward CW. Malformed mdx myofibers have normal cytoskeletal architecture yet altered EC coupling and stress-induced Ca2+ signaling. Am J Physiol Cell Physiol. 2009; 297:C571–C580. [PubMed: 19605736]
29. Gee SH, Madhavan R, Levinson SR, Caldwell JH, Sealock R, Froehner SC. Interaction of muscle and brain sodium channels with multiple members of the syntrophin family of dystrophin-associated proteins. J Neurosci. 1998; 18:128–137. [PubMed: 9412493]
30. Kong J, Anderson JE. Dystrophin is required for organizing large acetylcholine receptor aggregates. Brain Res. 1999; 839:298–304. [PubMed: 10519053]
31. Pratt SJ, Shah SB, Ward CW, Inacio MP, Stains JP, Lovering RM. Effects of in vivo injury on the neuromuscular junction in healthy and dystrophic muscles. J Physiol. 2013; 591:559–570. [PubMed: 23109110]
32. Khairallah RJ, Shi G, Sbrana F, et al. Microtubules underlie dysfunction in duchenne muscular dystrophy. Sci Signal. 2012; 5:ra56. [PubMed: 22871609]
33. Whitehead NP, Yeung EW, Allen DG. Muscle damage in mdx (dystrophic) mice: role of calcium and reactive oxygen species. Clin Exp Pharmacol Physiol. 2006; 33:657–662. [PubMed: 16789936]
34. Franklin, KBJ.; Paxinos, G. The mouse brain in stereotaxic coordinates. 3. 2007.
35. Xu S, Ji Y, Chen X, Yang Y, Gullapalli RP, Masri R. In vivo high-resolution localized (1) H MR spectroscopy in the awake rat brain at 7 T. Magn Reson Med. 2013; 69:937–943. [PubMed: 22570299]
36. Provencher SW. Automatic quantitation of localized in vivo 1H spectra with LCModel. NMR Biomed. 2001; 14:260–264. [PubMed: 11410943]
37. Zhuo J, Xu S, Proctor JL, et al. Diffusion kurtosis as an in vivo imaging marker for reactive astrogliosis in traumatic brain injury. Neuroimage. 2012; 59:467–477. [PubMed: 21835250]
38. Golmohammadi MG, Blackmore DG, Large B, et al. Comparative analysis of the frequency and distribution of stem and progenitor cells in the adult mouse brain. Stem Cells. 2008; 26:979–987. [PubMed: 18203672]
39. Petrof BJ. Molecular pathophysiology of myofiber injury in deficiencies of the dystrophin-glycoprotein complex. Am J Phys Med Rehabil. 2002; 81:S162–S174. [PubMed: 12409821]
40. Rando TA. The dystrophin-glycoprotein complex, cellular signaling, and the regulation of cell survival in the muscular dystrophies. Muscle Nerve. 2001; 24:1575–1594. [PubMed: 11745966]
41. Muntoni F, Torelli S, Ferlini A. Dystrophin and mutations: one gene, several proteins, multiple phenotypes. Lancet Neurol. 2003; 2:731–740. [PubMed: 14636778]
42. Garcia-Tovar CG, Perez A, Luna J, et al. Biochemical and histochemical analysis of 71 kDa dystrophin isoform (Dp71f) in rat brain. Acta Histochem. 2001; 103:209–224. [PubMed: 11368101]
43. Daoud F, Angeard N, Demerre B, et al. Analysis of Dp71 contribution in the severity of mental retardation through comparison of Duchenne and Becker patients differing by mutation consequences on Dp71 expression. Hum Mol Genet. 2009; 18:3779–3794. [PubMed: 19602481]
44. Moizard MP, Toutain A, Fournier D, et al. Severe cognitive impairment in DMD: obvious clinical indication for Dp71 isoform point mutation screening. Eur J Hum Genet. 2000; 8:552–556. [PubMed: 10909857]
45. Taylor PJ, Betts GA, Maroulis S, et al. Dystrophin gene mutation location and the risk of cognitive impairment in Duchenne muscular dystrophy. PLoS One. 2010; 5:e8803. [PubMed: 20098710]
46. Lenk U, Hanke R, Thiele H, Speer A. Point mutations at the carboxy terminus of the human dystrophin gene: implications for an association with mental retardation in DMD patients. Hum Mol Genet. 1993; 2:1877–1881. [PubMed: 8281150]
47. Culligan K, Ohlendieck K. Diversity of the Brain Dystrophin-Glycoprotein Complex. J Biomed Biotechnol. 2002; 2:31–36. [PubMed: 12488597]
48. Lidov HG, Byers TJ, Watkins SC, Kunkel LM. Localization of dystrophin to postsynaptic regions of central nervous system cortical neurons. Nature. 1990; 348:725–728. [PubMed: 2259381]
49. Kim TW, Wu K, Xu JL, Black IB. Detection of dystrophin in the postsynaptic density of rat brain and deficiency in a mouse model of Duchenne muscular dystrophy. Proc Natl Acad Sci U S A. 1992; 89:11642–11644. [PubMed: 1454857]

50. Nico B, Frigeri A, Nicchia GP, et al. Severe alterations of endothelial and glial cells in the blood-brain barrier of dystrophic mdx mice. Glia. 2003; 42:235–251. [PubMed: 12673830]
51. Goodnough CL, Gao Y, Li X, et al. Lack of dystrophin results in abnormal cerebral diffusion and perfusion in vivo. Neuroimage. 2014; 102(Pt 2):809–816. [PubMed: 25213753]
52. Warskulat U, Flogel U, Jacoby C, et al. Taurine transporter knockout depletes muscle taurine levels and results in severe skeletal muscle impairment but leaves cardiac function uncompromised. FASEB J. 2004; 18:577–579. [PubMed: 14734644]
53. Huxtable RJ. Physiological actions of taurine. Physiol Rev. 1992; 72:101–163. [PubMed: 1731369]
54. Conte CD, Tricarico D, Pierno S, et al. Taurine and skeletal muscle disorders. Neurochem Res. 2004; 29:135–142. [PubMed: 14992272]
55. Hollingworth S, Zeiger U, Baylor SM. Comparison of the myoplasmic calcium transient elicited by an action potential in intact fibres of mdx and normal mice. J Physiol. 2008; 586:5063–5075. [PubMed: 18772198]
56. Woods CE, Novo D, DiFranco M, Vergara JL. The action potential-evoked sarcoplasmic reticulum calcium release is impaired in mdx mouse muscle fibres. J Physiol. 2004; 557:59–75. [PubMed: 15004213]
57. Yeung EW, Whitehead NP, Suchyna TM, Gottleib PA, Sachs F, Allen DG. Effects of stretch-activated channel blockers on [Ca2+]i and muscle damage in the mdx mouse. J Physiol. 2004
58. Hernandez-Ochoa EO, Pratt SJ, Garcia-Pelagio KP, Schneider MF, Lovering RM. Disruption of action potential and calcium signaling properties in malformed myofibers from dystrophin-deficient mice. Physiol Rep. 2015; 3
59. Woods CE, Novo D, DiFranco M, Capote J, Vergara JL. Propagation in the transverse tubular system and voltage dependence of calcium release in normal and mdx muscle fibres. J Physiol. 2005
60. Friedrich O, von WF, Chamberlain JS, Fink RH, Rohrbach P. L-type Ca2+ channel function is linked to dystrophin expression in mammalian muscle. PLoS One. 2008; 3:e1762. [PubMed: 18516256]
61. Yeung EW, Whitehead NP, Suchyna TM, Gottlieb PA, Sachs F, Allen DG. Effects of stretch-activated channel blockers on [Ca2+]i and muscle damage in the mdx mouse. J Physiol. 2005; 562:367–380. [PubMed: 15528244]
62. Kar NC, Pearson CM. Catalase, superoxide dismutase, glutathione reductase and thiobarbituric acid-reactive products in normal and dystrophic human muscle. Clin Chim Acta. 1979; 94:277–280. [PubMed: 466816]
63. Mizuno Y. Changes in superoxide dismutase, catalase, glutathione peroxidase, and glutathione reductase activities and thiobarbituric acid-reactive products levels in early stages of development in dystrophic chickens. Exp Neurol. 1984; 84:58–73. [PubMed: 6705887]
64. Murphy ME, Kehrer JP. Activities of antioxidant enzymes in muscle, liver and lung of chickens with inherited muscular dystrophy. Biochem Biophys Res Commun. 1986; 134:550–556. [PubMed: 3947339]
65. Rae C, Griffin JL, Blair DH, et al. Abnormalities in brain biochemistry associated with lack of dystrophin: studies of the mdx mouse. Neuromuscul Disord. 2002; 12:121–129. [PubMed: 11738353]
66. Kanfer JN, McCartney DG. Reduced phosphorylcholine hydrolysis by homogenates of temporal regions of Alzheimer's brain. Biochem Biophys Res Commun. 1986; 139:315–319. [PubMed: 3767960]
67. Pettegrew JW, Moossy J, Withers G, McKeag D, Panchalingam K. 31P nuclear magnetic resonance study of the brain in Alzheimer's disease. J Neuropathol Exp Neurol. 1988; 47:235–248. [PubMed: 3367156]
68. Sok DE. Oxidative inactivation of brain alkaline phosphatase responsible for hydrolysis of phosphocholine. J Neurochem. 1999; 72:355–362. [PubMed: 9886088]
69. Reggiani C. Between channels and tears: aim at ROS to save the membrane of dystrophic fibres. J Physiol. 2008; 586:1779. [PubMed: 18381339]

70. Knuesel I, Mastrocola M, Zuellig RA, Bornhauser B, Schaub MC, Fritschy JM. Short communication: altered synaptic clustering of GABAA receptors in mice lacking dystrophin (mdx mice). Eur J Neurosci. 1999; 11:4457–4462. [PubMed: 10594673]

71. Goyenvalle A, Griffith G, Babbs A, et al. Functional correction in mouse models of muscular dystrophy using exon-skipping tricyclo-DNA oligomers. Nat Med. 2015; 21:270–275. [PubMed: 25642938]

72. Chamberlain JS, Metzger J, Reyes M, Townsend D, Faulkner JA. Dystrophin-deficient mdx mice display a reduced life span and are susceptible to spontaneous rhabdomyosarcoma. FASEB J. 2007; 21:2195–2204. [PubMed: 17360850]

73. Glesby MJ, Rosenmann E, Nylen EG, Wrogemann K. Serum CK, calcium, magnesium, and oxidative phosphorylation in mdx mouse muscular dystrophy. Muscle Nerve. 1988; 11:852–856. [PubMed: 3173410]

74. Muntoni F, Mateddu A, Marchei F, Clerk A, Serra G. Muscular weakness in the mdx mouse. J Neurol Sci. 1993; 120:71–77. [PubMed: 8289081]

75. De la PS, Morin S, Koenig J. Characteristics of skeletal muscle in mdx mutant mice. Int Rev Cytol. 1999; 191:99–148. [PubMed: 10343393]

76. Dangain J, Vrbova G. Muscle development in mdx mutant mice. Muscle Nerve. 1984; 7:700–704. [PubMed: 6543918]

77. Dubowitz V, Crome L. The central nervous system in Duchenne muscular dystrophy. Brain. 1969; 92:805–808. [PubMed: 5364010]

78. Bresolin N, Castelli E, Comi GP, et al. Cognitive impairment in Duchenne muscular dystrophy. Neuromuscul Disord. 1994; 4:359–369. [PubMed: 7981593]

79. Schmidt B, Watters GV, Rosenblatt B, Silver K. Increased head circumference in patients with Duchenne muscular dystrophy. Ann Neurol. 1985; 17:620–621. [PubMed: 4026239]

80. Appleton RE, Bushby K, Gardner-Medwin D, Welch J, Kelly PJ. Head circumference and intellectual performance of patients with Duchenne muscular dystrophy. Dev Med Child Neurol. 1991; 33:884–890. [PubMed: 1743411]

81. Rosman NP, Kakulas BA. Mental deficiency associated with muscular dystrophy. A neuropathological study. Brain. 1966; 89:769–788. [PubMed: 4163581]

82. Rosman NP. The cerebral defect and myopathy in Duchenne muscular dystrophy. A comparative clinicopathological study. Neurology. 1970; 20:329–335. [PubMed: 5534965]

83. Septien L, Gras P, Borsotti JP, Giroud M, Nivelon JL, Dumas R. Mental development in Duchenne muscular dystrophy. Correlation of data of the brain scanner. Pediatrie. 1991; 46:817–819. [PubMed: 1667037]

84. al-Qudah AA, Kobayashi J, Chuang S, Dennis M, Ray P. Etiology of intellectual impairment in Duchenne muscular dystrophy. Pediatr Neurol. 1990; 6:57–59. [PubMed: 2310438]

85. Ortiz JG, Negron AE, Garcia MT, Rosado JE, Maldonaldo CS. The C57BL/10Bg sps/sps mouse: a mutant with absence-like seizures; neurochemical and behavioral correlates. Neurosci Lett. 1990; 114:231–236. [PubMed: 2395534]

86. Kueh SL, Dempster J, Head SI, Morley JW. Reduced postsynaptic GABAA receptor number and enhanced gaboxadol induced change in holding currents in Purkinje cells of the dystrophin-deficient mdx mouse. Neurobiol Dis. 2011; 43:558–564. [PubMed: 21601636]

Highlights

- Structure/metabolites of healthy and dystrophic (*mdx*) mouse brains were studied with MRI/MRS.
- MRI revealed enlarged lateral ventricles in *mdx* brains.
- DTI showed alterations in diffusion in the *mdx* prefrontal cortex and hippocampus.
- MRS indicated several metabolic alterations for *mdx* brains.
- The brain lacking dystrophin has structural changes and multiple brain dysfunctions.

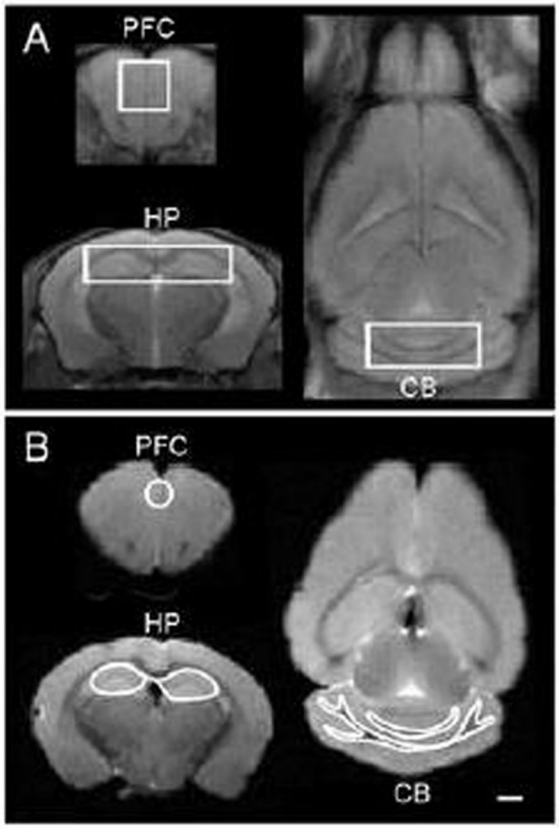

Figure 1.

A: *In vivo* proton-density-weighted MR images showing regions of interest (ROI) for *in vivo* ^{1}H MRS experiments. **B**: *Ex vivo* proton-density-weighted MR images showing the placement of the brain regions of interest of DTI experiments. PFC = prefrontal cortex; HP = hippocampus; CB = cerebellum. Scale bar = 1 mm

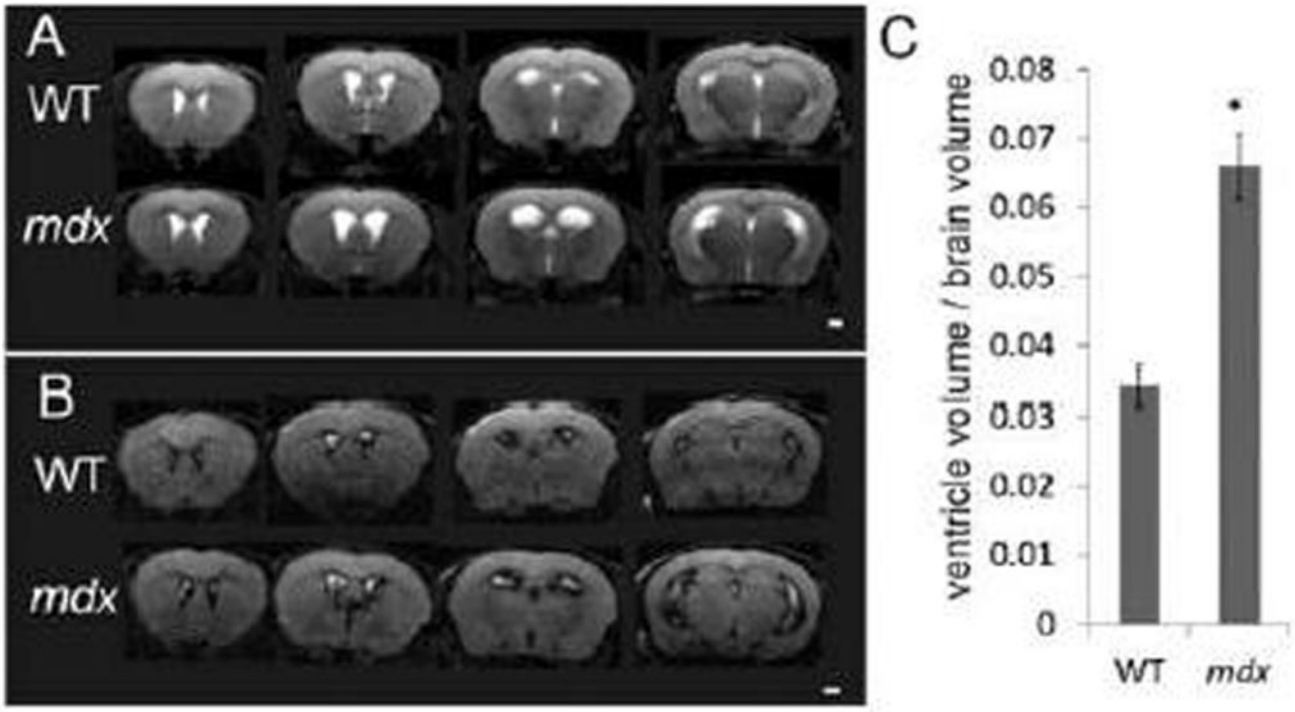

Figure 2.

A: Representative *in vivo* T_2-weighted coronal MR images from a WT mouse (top row) and an *mdx* (bottom row) mouse. **B**: Representative *in vivo* fluid-attenuated inversion recovery (FLAIR) coronal MR images from a WT mouse (top row) and an *mdx* mouse (bottom row). Excess cerebrospinal fluid displayed by the high signal intensity (bright white) on the T_2-weighed images (A) and low signal intensity (dark black) on the FLAIR images (B). **C**: Comparison of the ventricle/whole brain tissue volume from the T_2-weighted MRI images between WT and *mdx* mice. Data are expressed as mean ± standard error, * $p < 0.05$ ($p = 0.0001$). Scale bar = 1 mm

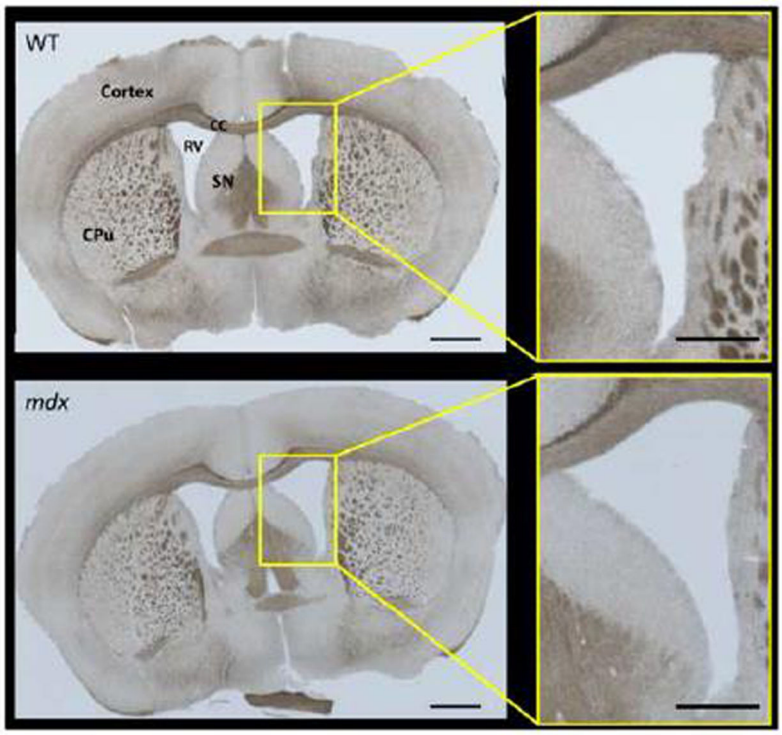

Figure 3.

Representative sections of brain from WT and *mdx* mice. Gross morphology was similar in both groups (N = 2 per group), but the changes in ventricle size seen with imaging (Fig. 2) were also apparent with histological imaging. CC = corpus callosum, CPu = caudate putamen, RV = right ventricle, SN = septal nucleus. Image scale bars = 1000 μm. Panel inset scale bars = 500 μm.

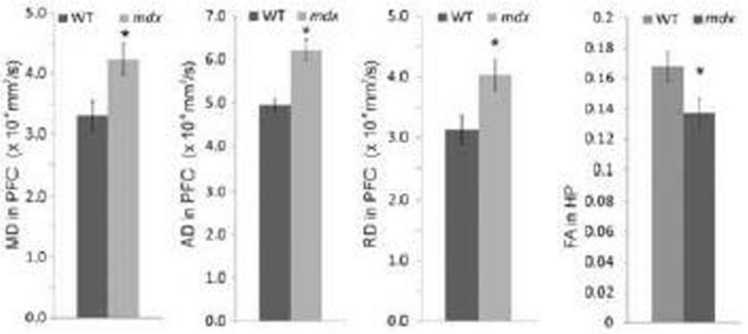

Figure 4.

Comparison of the water diffusion characters between WT and *mdx* mice in prefrontal cortex (PFC) and hippocampus (HP). MD = mean diffusivity; RD = radial diffusivity; AD = axial diffusivity; FA = fractional anisotropy (relative units). Data are derived from brains *ex vivo* and expressed as mean ± standard error, * $p < 0.05$

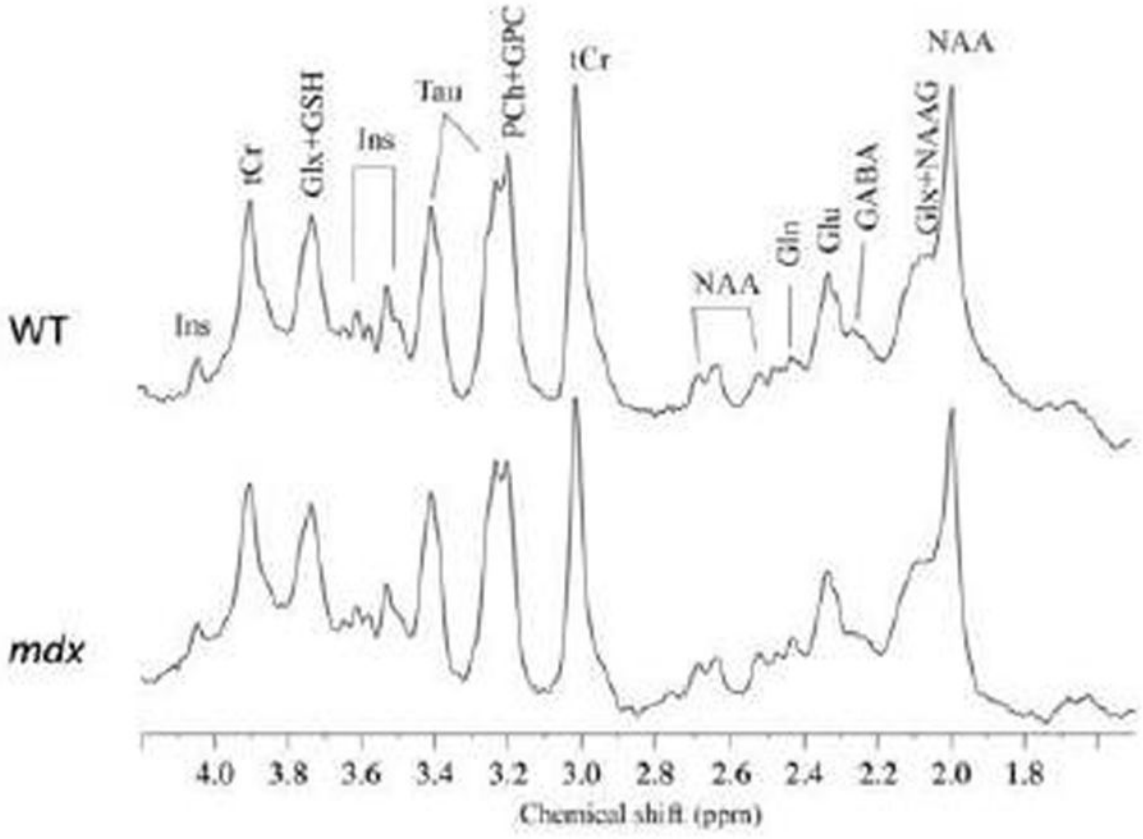

Figure 5.

Representative *in vivo* ^{1}H MR spectra at 7 Tesla from the hippocampus from a WT mouse and an *mdx* mouse. γ-aminobutyric acid (GABA), glutamine (Gln), glutamate (Glu), glutathione (GSH), *myo*-inositol (Ins), *N*-acetylaspartate (NAA), *N*-acetylaspartateglutamate (NAAG), taurine (Tau), total creatine (tCr), phosphocholine (PCh), glycerophosphocholine (GPC), and glutamate/glutamine complex (Glx).

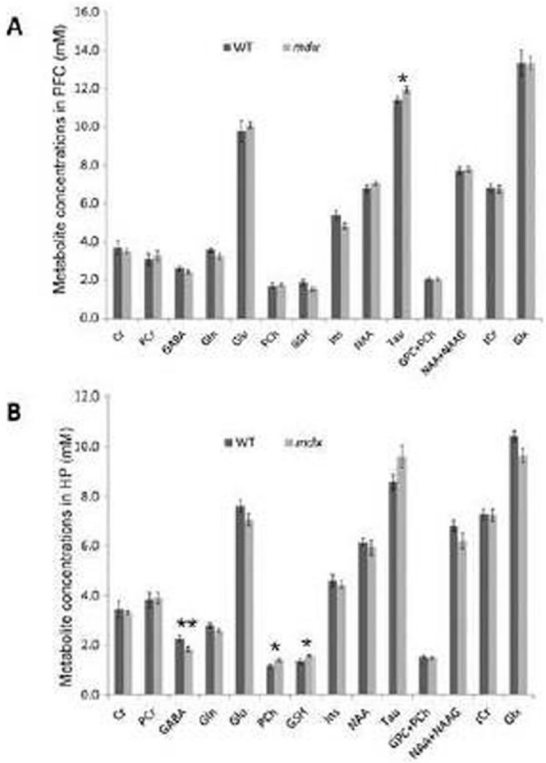

Figure 6.

Comparison of the neurometabolic concentration (mM) between WT and *mdx* mice in prefrontal cortex (PFC, A) and hippocampus (HP, B). Data are expressed as mean ± standard error. * $p < 0.05$; ** $p < 0.01$.